GEOPHYSICS, VOL. 72, NO. 5 (SEPTEMBER-OCTOBER 2007); P. SM155–SM167, 10 FIGS., 1 TABLE.
10.1190/1.2757586

An unsplit convolutional perfectly matched layer improved at grazing incidence for the seismic wave equation

Dimitri Komatitsch[1] and Roland Martin[1]

ABSTRACT

The perfectly matched layer (PML) absorbing boundary condition has proven to be very efficient from a numerical point of view for the elastic wave equation to absorb both body waves with nongrazing incidence and surface waves. However, at grazing incidence the classical discrete PML method suffers from large spurious reflections that make it less efficient for instance in the case of very thin mesh slices, in the case of sources located close to the edge of the mesh, and/or in the case of receivers located at very large offset. We demonstrate how to improve the PML at grazing incidence for the differential seismic wave equation based on an unsplit convolution technique. The improved PML has a cost that is similar in terms of memory storage to that of the classical PML. We illustrate the efficiency of this improved convolutional PML based on numerical benchmarks using a finite-difference method on a thin mesh slice for an isotropic material and show that results are significantly improved compared with the classical PML technique. We also show that, as the classical PML, the convolutional technique is intrinsically unstable in the case of some anisotropic materials.

INTRODUCTION

Because of the very rapid increase of computational power, the development of methods for the numerical simulation of seismic wave propagation in complex geologic media has been the subject of a continuous effort during the past three decades. Different approaches are available to solve the seismic wave equation in such models. Among the most popular are the finite-difference method (e.g., Alterman and Karal, 1968; Madariaga, 1976; Virieux, 1986), spectral and pseudo-spectral techniques (e.g., Carcione, 1994; Tessmer and Kosloff, 1994), boundary-element or boundary-integral methods (Kawase, 1988; Sánchez-Sesma and Campillo, 1991), finite-element methods (e.g., Lysmer and Drake, 1972; Marfurt, 1984; Bao et al., 1998), and spectral-element methods (e.g., Cohen et al., 1993; Priolo et al., 1994; Faccioli et al., 1997; Komatitsch and Vilotte, 1998; Komatitsch and Tromp, 1999; Chaljub et al., 2003). More recently, discontinuous Galerkin formulations have also been used (e.g., Dumbser and Käser, 2006).

In the context of numerical modeling of seismic wave propagation in unbounded media, as in the case of simulations performed at the local, regional, or continental scale, energy needs to be absorbed at the artificial boundaries of the computational domain and therefore nonreflecting conditions must be defined at these boundaries to mimic an unbounded medium. In the last 30 years, numerous techniques have been developed for this purpose: damping layers or sponge zones (e.g., Cerjan et al., 1985; Sochacki et al., 1987), paraxial conditions (e.g., Clayton and Engquist, 1977; Engquist and Majda, 1977; Stacey, 1988; Higdon, 1991; Quarteroni et al., 1998), optimized conditions (e.g., Peng and Töksoz, 1995), the eigenvalue decomposition method (e.g., Dong et al., 2005), continued fraction absorbing conditions (e.g., Guddati and Lim, 2006), exact absorbing conditions on a spherical contour (e.g., Grote, 2000), or asymptotic local or nonlocal operators (e.g., Givoli, 1991; Hagstrom and Hariharan, 1998). However, all of the local conditions exhibit poor behavior under some circumstances. For instance, they typically reflect a large amount of spurious energy at grazing incidence or low-frequency energy at all angles of incidence, and nonlocal conditions are difficult to implement and numerically expensive. In the context of Maxwell's equations, Bérenger (1994) introduced a new condition called the perfectly matched layer (PML) that has the remarkable property of having a zero reflection coefficient for all angles of incidence and all frequencies before discretization (hence the name perfectly matched). This formulation has proven to be more efficient compared with classical conditions and has become widely used. The formulation was rapidly extended to 3D problems (e.g., Chew and Weedon, 1994; Bérenger, 1996) and reformulated in a simpler way in terms of a split field with complex coordinate stretching (e.g., Chew and Weedon, 1994; Collino and Monk, 1998b). The PML is now routinely used in many other fields, e.g., linearized Euler equa-

Manuscript received by the Editor December 5, 2006; revised manuscript received March 13, 2007; published online August 23, 2007.
[1]Université de Pau et des Pays de l'Adour, Laboratoire de Modélisation et d'Imagerie en Géosciences, CNRS UMR 5212 & INRIA Futurs Magique-3D, Pau, France. E-mail: dimitri.komatitsch@univ-pau.fr; roland.martin@univ-pau.fr.

tions (Hesthaven, 1998), eddy-current problems (Kosmanis et al., 1999), and wave propagation in poroelastic media (Zeng et al., 2001).

Regarding seismic wave propagation, the PML has been successfully applied to both acoustic (e.g., Liu and Tao, 1997; Qi and Geers, 1998; Abarbanel et al., 1999; Katsibas and Antonopoulos, 2002; Diaz and Joly, 2006; Bermúdez et al., 2007) and elastic problems (e.g., Chew and Liu, 1996; Hastings et al., 1996; Collino and Tsogka, 2001; Festa and Nielsen, 2003; Komatitsch and Tromp, 2003; Basu and Chopra, 2004; Rahmouni, 2004; Cohen and Fauqueux, 2005; Festa and Vilotte, 2005; Festa et al., 2005; Appelö and Kreiss, 2006; Ma and Liu, 2006). Collino and Tsogka (2001) illustrate the high efficiency of the condition compared with the paraxial treatment of Higdon (1991), even though the PML reflection coefficient is not exactly zero after discretization (e.g., Collino and Monk, 1998a). Compared with other conditions (for instance paraxial equations) that are designed to absorb body waves, but that behave poorly for surface waves, the PML has the additional advantage of being highly efficient for the absorption of such surface waves (Collino and Tsogka, 2001; Komatitsch and Tromp, 2003; Festa et al., 2005).

A classical PML for the seismic wave equation is naturally formulated in terms of velocity and stress, i.e., for a system of first-order equations in time (e.g., Collino and Tsogka, 2001; Komatitsch and Tromp, 2003). Unfortunately, this means that it cannot be used directly in numerical schemes that are based on the wave equation written as a second-order system in displacement, such as most finite-element methods (e.g., Bao et al., 1998), most spectral-element methods (e.g., Komatitsch and Vilotte, 1998; Komatitsch and Tromp, 1999), and some finite-difference methods (e.g., Moczo et al., 2001). Therefore, in recent years efforts have been made to derive PML formulations suitable for such a second-order system written in displacement: Komatitsch and Tromp (2003) and Basu and Chopra (2004) derived formulations of the PML that are directly adapted to second-order equations, Festa and Vilotte (2005) show that the classical first-order PML formulation can be used as it is based upon a discrete equivalence between the Newmark time-stepping method and the midpoint rule applied to a staggered velocity-stress system, and Cohen and Fauqueux (2005) chose the alternative approach of adapting the spectral-element method to the PML by constructing a spectral-element formulation based on the mixed velocity-stress system, which is well suited to the introduction of PML. Another approach consists of writing the PML system based on an integral term in time and computing the integral using the trapezoidal rule (e.g., Zeng et al., 2001, Wang and Tang, 2003; Festa and Vilotte, 2005) but the overall accuracy of this approach could deserve further study because the trapezoidal rule is exact for polynomials of degree 1 only.

A recurring problem in the context of the use of a discrete PML model for Maxwell's equations or for the equations of elastodynamics is that the reflection coefficient is not zero after discretization, but more importantly that it becomes very large at grazing incidence (e.g., Collino and Monk, 1998a; Winton and Rappaport, 2000). In this case, a large amount of energy is sent back into the main domain in the form of spurious reflected waves. This makes the classical PML less efficient for instance in the case of thin mesh slices, or in the case of sources located close to the edge of the mesh, or receivers located at very large offset, which are situations that are rather common, for example in oil industry simulations. To overcome this problem, Collino and Monk (1998a) calculate the analytical expression of the numerical reflection coefficient of a discrete scheme for Maxwell's equations for the classical 2D staggered finite-difference grid of Yee (1966) and sum the values of this discrete coefficient for various angles of incidence (by steps of 1° between normal incidence and grazing incidence). They then use a least-squares algorithm to optimize the discrete damping profile at each point of the finite-difference grid in the PML layer to globally minimize the amount of energy sent back into the medium, which means making discrete PML absorption less efficient near normal incidence, where it is already almost perfect, to make it more efficient at grazing incidence, where it is poor. Fontes (2006) tried to use the same approach for the elastic wave equation by calculating the analytical expression of the four discrete reflection coefficients: *Rpp*, *Rps*, *Rsp*, and *Rss* for the classical 2D staggered finite-difference grid of Madariaga (1976) and Virieux (1986) to be able to then use a least-squares technique to globally minimize the amount of energy sent back into the main domain in the form of spurious P- and/or S-waves, this for all the range of possible angles of incidence by sampling this range every degree between 1° and 90°. He gave up this approach because the situation in elastodynamics is more complicated than for Maxwell's equations studied by Collino and Monk (1998a) because there are two types of body waves (P and S) and thus four discrete reflection coefficients, and it is therefore not easy to decide which coefficient to optimize, nor to make sure that optimizing one of them will not degrade the others. It is difficult to plan to optimize the four coefficients simultaneously because one does not control the quantity of energy that arrives on a PML edge independently in the form of plane P- and S-waves. We could think of optimizing the arithmetic mean of the four coefficients, but this is not realistic from a geophysical point of view because the quantity of energy arriving on the edge of the medium in the form of P- and S-waves strongly depends on the radiation pattern of the seismic source and on the geologic medium considered, and therefore such an optimization would not be possible independently of the medium under study. Moreover such an analysis does not include surface waves, which often carry a large amount of energy.

Another approach to improve the behavior of the discrete PML at grazing incidence consists in modifying the complex coordinate transform used classically in the PML (see next section) to introduce a frequency-dependent term (Kuzuoglu and Mittra, 1996) that implements a Butterworth-type filter in the layer. This approach has been developed for Maxwell's equations by Kuzuoglu and Mittra (1996) and Roden and Gedney (2000) and named convolutional-PML (C-PML) or complex frequency shifted-PML (CFS-PML) (Bérenger, 2002a, b). The key idea is that for waves whose incidence is close to normal, the presence of such a filter changes almost nothing because absorption is already almost perfect. But for waves with grazing incidence, which for geometrical reasons do not penetrate very deep in the PML, but travel there a longer way in the direction parallel to the layer, adding such a filter will strongly attenuate them and will prevent them from leaving the PML with significant energy. In this study, we adapt this approach to the equations of elastodynamics. Let us note that a similar idea called the generalized filtering-PML was used recently in elastodynamics (Festa and Vilotte, 2005) in the context of a variational formulation based on the spectral-element method. However, that implementation is based, like the original formulations of Bérenger (1994) and Collino and Tsogka (2001), on a split formulation of the equations of elastodynamics. The formulation that we introduce has the advantage of not being split. Its cost in terms of memory storage is similar to that of the classical PML.

CLASSICAL PML FORMULATION IN VELOCITY AND STRESS

The differential or strong form of the anisotropic elastic wave equation can be written as

$$\rho\partial_t^2\mathbf{s} = \nabla\cdot(\mathbf{c}\colon\nabla\mathbf{s}), \tag{1}$$

where $\mathbf{s} = \mathbf{s}(\mathbf{x},t)$ is the displacement vector, $\mathbf{c}$ the full elastic tensor with up to 21 independent coefficients, and ρ the density. The frequency-domain form of this equation is

$$-\rho\omega^2\mathbf{s} = \nabla\cdot(\mathbf{c}\colon\nabla\mathbf{s}), \tag{2}$$

where ω denotes angular frequency and where, for simplicity, we have used the same notation $\mathbf{s} = \mathbf{s}(\mathbf{x},\omega)$ for the displacement vector in the frequency domain. We will use the same notation in both domains for other variables in the rest of this article. In the particular case of a homogeneous medium, this equation has plane wave solutions of the form $\mathbf{A}\exp(-\mathrm{i}(\mathbf{k}\cdot\mathbf{x}-\omega t))$, where $\mathbf{A}$ represents the amplitude and polarization of the plane wave, $\mathbf{k} = k_x\hat{\mathbf{x}} + k_y\hat{\mathbf{y}} + k_z\hat{\mathbf{z}}$ its wave vector with Cartesian components k_x, k_y, and k_z, and $\mathbf{x} = x\hat{\mathbf{x}} + y\hat{\mathbf{y}} + z\hat{\mathbf{z}}$ the position vector. In the case of an isotropic medium, for plane P-waves $\mathbf{A}\times\mathbf{k} = \mathbf{0}$ and $k = (k_x^2 + k_y^2 + k_z^2)^{1/2} = \omega/\alpha$, where α denotes the P-wave velocity, whereas for plane S-waves $\mathbf{A}\cdot\mathbf{k} = 0$ and $k = \omega/\beta$, where β denotes the S-wave velocity.

Following the discussions in Chew and Weedon (1994), Collino and Monk (1998a), Teixeira and Chew (1999), and Collino and Tsogka (2001), to which the reader is referred for more details, the PML can be viewed as an analytical continuation of the real coordinates in the complex space. Let us consider a PML layer located at $x > 0$ and the regular domain located at $x \le 0$ (Figure 1). One first defines a damping profile $d_x(x)$ in the PML region, such that $d_x = 0$ inside the main domain (i.e., outside the PML) and $d_x > 0$ in the PML. Let us note that subscript x is just a label for the x-axis, whereas argument x is a real variable. A new complex coordinate $\tilde{x}$ is then introduced and expressed in terms of this damping profile as:

$$\tilde{x}(x) = x - \frac{\mathrm{i}}{\omega}\int_0^x d_x(s)\mathrm{d}s \tag{3}$$

or, equivalently, upon differentiating

$$\partial_{\tilde{x}} = \frac{\mathrm{i}\omega}{\mathrm{i}\omega + d_x}\partial_x = \frac{1}{s_x}\partial_x, \tag{4}$$

with

$$s_x = \frac{\mathrm{i}\omega + d_x}{\mathrm{i}\omega} = 1 + \frac{d_x}{\mathrm{i}\omega}. \tag{5}$$

The goal is now to change the original equation 1 written in terms of variables x, y, and z, into a new wave equation written in terms of variables $\tilde{x}$, y, and z. To do this, let us denote by $\hat{\mathbf{n}}$ the normal to the interface between the model and the PML region. The gradient operator ∇ can be split in terms of components perpendicular and parallel to the interface:

$$\nabla = \hat{\mathbf{n}}\partial_x + \nabla^{\parallel}. \tag{6}$$

Here $\partial_x = \hat{\mathbf{n}}\cdot\nabla$ and $\nabla^{\parallel} = (\mathbf{I} - \hat{\mathbf{n}}\hat{\mathbf{n}})\cdot\nabla$, where $\mathbf{I}$ is the 3×3 identity tensor, and $\mathbf{I} - \hat{\mathbf{n}}\hat{\mathbf{n}}$ is the projection operator onto the surface with normal $\hat{\mathbf{n}}$.

In the classical first-order velocity-stress formulation (e.g., Collino and Tsogka, 2001), one first rewrites equation 1 as

$$\begin{aligned}\rho\partial_t\mathbf{v} &= \nabla\cdot\sigma,\\ \partial_t\sigma &= \mathbf{c}\colon\nabla\mathbf{v},\end{aligned} \tag{7}$$

where $\mathbf{v}$ is the velocity vector and σ the second-order stress tensor. The frequency-domain form of this system of equations is

$$\begin{aligned}\mathrm{i}\omega\rho\mathbf{v} &= \nabla\cdot\sigma,\\ \mathrm{i}\omega\sigma &= \mathbf{c}\colon\nabla\mathbf{v}.\end{aligned} \tag{8}$$

Using equation 6, one gets

$$\begin{aligned}\mathrm{i}\omega\rho\mathbf{v} &= \hat{\mathbf{n}}\partial_x\cdot\sigma + \nabla^{\parallel}\cdot\sigma,\\ \mathrm{i}\omega\sigma &= \mathbf{c}\colon\hat{\mathbf{n}}\partial_x\mathbf{v} + \mathbf{c}\colon\nabla^{\parallel}\mathbf{v}.\end{aligned} \tag{9}$$

One then replaces the wave equation 9 written in terms of x with a generalized wave equation written in terms of $\tilde{x}$:

$$\begin{aligned}\mathrm{i}\omega\rho\mathbf{v} &= \hat{\mathbf{n}}\partial_{\tilde{x}}\cdot\sigma + \nabla^{\parallel}\cdot\sigma,\\ \mathrm{i}\omega\sigma &= \mathbf{c}\colon\hat{\mathbf{n}}\partial_{\tilde{x}}\mathbf{v} + \mathbf{c}\colon\nabla^{\parallel}\mathbf{v}.\end{aligned} \tag{10}$$

Inside the main domain, both equations are identical because $d_x = 0$. But in the PML, this modified wave equation has exponentially decaying plane wave solutions of the form:

$$\mathbf{A}e^{-\mathrm{i}(k_x\tilde{x}+k_yy+k_zz-\omega t)} = \mathbf{A}e^{-\mathrm{i}(\mathbf{k}\cdot\mathbf{x}-\omega t)}e^{-k_x/\omega\int_0^x d_x(s)\mathrm{d}s} \tag{11}$$

in the $\hat{\mathbf{n}}$ direction (i.e., the x-direction here) with a decay coefficient $\exp(-k_x/\omega\int_0^x d_x(s)\mathrm{d}s)$ that is inversely proportional to the angular frequency ω of the plane wave. Let us note that this damping coefficient depends on the direction of propagation of the wave, and is large for a wave propagating close to normal incidence, but becomes significantly smaller for a wave propagating at grazing incidence, which explains the reduced efficiency of the classical PML model at grazing incidence. Let us also note that the reflection coefficient between the medium and the PML region is exactly zero for all angles

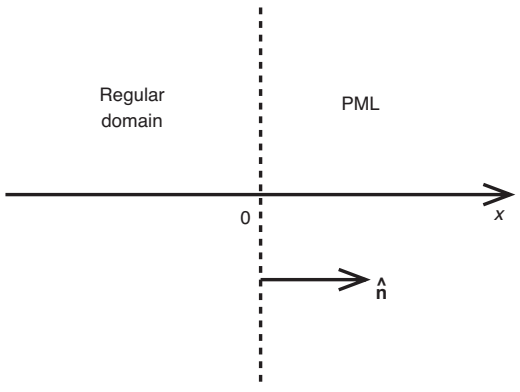

Figure 1. Definition of the main domain and the PML layer. The PML region starts at $x = 0$ and extends to $x > 0$. The local normal to the interface is denoted by $\hat{\mathbf{n}}$.

of incidence and all frequencies here, before discretization by a numerical scheme, hence the name perfectly matched layer. One then uses the mapping equation 4 to rewrite the wave equation 10 in terms of x rather than $\tilde{x}$:

$$\begin{aligned} \mathrm{i}\omega\rho\mathbf{v} &= \hat{\mathbf{n}}\frac{1}{s_x}\partial_x \cdot \sigma + \nabla^{\parallel} \cdot \sigma, \\ \mathrm{i}\omega\sigma &= \mathbf{c}{:}\hat{\mathbf{n}}\frac{1}{s_x}\partial_x\mathbf{v} + \mathbf{c}{:}\nabla^{\parallel}\mathbf{v}. \end{aligned} \tag{12}$$

The velocity and stress fields are then split into two parts (e.g., Chew and Weedon, 1994; Collino and Monk, 1998b; Collino and Tsogka, 2001), $\mathbf{v} = \mathbf{v}^1 + \mathbf{v}^2$ and $\sigma = \sigma^1 + \sigma^2$, such that

$$\begin{aligned} \mathrm{i}\omega\rho\mathbf{v}^1 &= \frac{1}{s_x}\hat{\mathbf{n}} \cdot \partial_x\sigma, \\ \mathrm{i}\omega\rho\mathbf{v}^2 &= \nabla^{\parallel} \cdot \sigma, \\ \mathrm{i}\omega\sigma^1 &= \mathbf{c}{:}\hat{\mathbf{n}}\frac{1}{s_x}\partial_x\mathbf{v}, \\ \mathrm{i}\omega\sigma^2 &= \mathbf{c}{:}\nabla^{\parallel}\mathbf{v}. \end{aligned} \tag{13}$$

Converting back to the time domain one finally gets

$$\begin{aligned} (\partial_t + d_x)\rho\mathbf{v}^1 &= \hat{\mathbf{n}}\partial_x \cdot \sigma, \\ \partial_t\rho\mathbf{v}^2 &= \nabla^{\parallel} \cdot \sigma, \\ (\partial_t + d_x)\sigma^1 &= \mathbf{c}{:}\hat{\mathbf{n}}\partial_x\mathbf{v}, \\ \partial_t\sigma^2 &= \mathbf{c}{:}\nabla^{\parallel}\mathbf{v}, \end{aligned} \tag{14}$$

which permits the desired exponentially decaying plane wave solutions of equation 11 and governs wave propagation in the classical first-order PML.

As mentioned in the introduction, there are two main drawbacks associated with this classical formulation: First it requires the use of split fields, and second, and more importantly, its efficiency becomes poor at grazing incidence after discretization. The first issue has been addressed in literature in the case of Maxwell's equations (e.g., Gedney, 1996; Veihl and Mittra, 1996; Zhao and Cangellaris, 1996; Sullivan, 1997; Bérenger, 2002b) or the elastic wave equation (e.g., Wang and Tang, 2003; Rahmouni, 2004; Drossaert and Giannopoulos, 2007b). The C-PML approach has been developed by Roden and Gedney (2000) in the case of Maxwell's equations to address both issues. In what follows, we introduce such an unsplit C-PML technique for elastodynamics, as presented in 3D by Martin et al. (2005) and Martin and Komatitsch (2006), and more recently in 2D by Drossaert and Giannopoulos (2007a).

THE C-PML TECHNIQUE TO IMPROVE THE DISCRETE PML MODEL AT GRAZING INCIDENCE

Let us now introduce the C-PML technique for the equations of elastodynamics written in differential form in velocity and stress, following the approach of Roden and Gedney (2000). The technique is based on the writing of the PML model in the form of a convolution in time and on the introduction of memory variables to not have to explicitly store all the past states of the medium to carry out the convolution, but rather to calculate this convolution in a recursive way as suggested in Luebbers and Hunsberger (1992) and improved in Roden and Gedney (2000). Let us note that the idea of using memory variables is rather similar to that used in numerical modeling in geophysics to implement viscoelasticity in the seismic wave equation (e.g., Carcione et al., 1988; Day, 1998). Let us note that, as opposed to the traditional scheme of Collino and Tsogka (2001), this approach has the advantage of not being split, i.e., its implementation in existing finite-difference codes (without PML) is slightly easier because terms within the equations do not need to be split into separate equations, though extra memory terms have to be added. Indeed, as we do not need to split the unknowns $\mathbf{v}$ and σ, there is no need to modify the structure of the loops computing these arrays. It is sufficient to add an array to store each of these memory variables (in the PML layer only and not in the main domain, in which the damping coefficient is zero) and a loop to update each memory variable, which is straightforward.

The main idea of the C-PML technique consists of making a choice for s_x more general (Kuzuoglu and Mittra, 1996; Roden and Gedney, 2000; Bérenger, 2002a, b) than that of equation 5 by introducing not only the damping profile d_x, but also two other real variables $\alpha_x \geq 0$ and $\kappa_x \geq 1$ such that:

$$s_x = \kappa_x + \frac{d_x}{\alpha_x + \mathrm{i}\omega}. \tag{15}$$

In the particular case of $\kappa_x = 1$ and $\alpha_x = 0$, we get the classical PML coordinate transformation. As this expression depends on frequency, when we go back to the time domain we get a time convolution on each modified spatial derivative. Denoting by $\overline{s}_x(t)$ the inverse Fourier transform (labeled an inverse Laplace transform in Roden and Gedney [2000]) of $1/s_x$, ∂_x is replaced with (Roden and Gedney, 2000):

$$\partial_{\tilde{x}} = \overline{s}_x(t) * \partial_x. \tag{16}$$

Rewriting equation 15 as

$$\frac{1}{s_x} = \frac{1}{\kappa_x} - \frac{d_x}{\kappa_x^2}\frac{1}{(d_x/\kappa_x + \alpha_x) + \mathrm{i}\omega} \tag{17}$$

and noting that the Fourier transform of δ is 1 and that the Fourier transform of $e^{-at}H(t)$ is $1/(a + \mathrm{i}\omega)$ we get the value of $\overline{s}_x$:

$$\overline{s}_x(t) = \frac{\delta(t)}{\kappa_x} - \frac{d_x}{\kappa_x^2}H(t)e^{-(d_x/\kappa_x+\alpha_x)t}, \tag{18}$$

where $\delta(t)$ and $H(t)$ denote the Dirac delta and Heaviside distributions, respectively. If we denote:

$$\zeta_x(t) = -\frac{d_x}{\kappa_x^2}H(t)e^{-(d_x/\kappa_x+\alpha_x)t}, \tag{19}$$

we see that ∂_x is finally transformed in:

$$\partial_{\tilde{x}} = \frac{1}{\kappa_x}\partial_x + \zeta_x(t) * \partial_x. \tag{20}$$

The first of these two terms is easy to handle in an existing numerical code: One simply needs to divide the computed spatial derivative by κ_x. To compute the second term in the context of a discrete staggered time scheme, let us assume that we have discretized the time in N time steps of equal duration Δt. The convolution term computed at

time step n, which we will denote ψ_x^n in the following for convenience, can then be written:

$$\psi_x^n = (\zeta_x * \partial_x)^n = \int_0^{n\Delta t} (\partial_x)^{n\Delta t - \tau} \zeta_x(\tau) \mathrm{d}\tau. \quad (21)$$

Because the time integration scheme is staggered, ∂_x is defined half a time step between $m\Delta t$ and $(m+1)\Delta t$ and we can therefore write:

$$\begin{aligned}\psi_x^n &= \sum_{m=0}^{n-1} \int_{m\Delta t}^{(m+1)\Delta t} (\partial_x)^{n\Delta t - \tau} \zeta_x(\tau) \mathrm{d}\tau \\ &= \sum_{m=0}^{n-1} (\partial_x)^{n-(m+1/2)} \int_{m\Delta t}^{(m+1)\Delta t} \zeta_x(\tau) \mathrm{d}\tau \\ &= \sum_{m=0}^{n-1} Z_x(m) (\partial_x)^{n-(m+1/2)}, \end{aligned} \quad (22)$$

with:

$$Z_x(m) = \int_{m\Delta t}^{(m+1)\Delta t} \zeta_x(\tau) \mathrm{d}\tau. \quad (23)$$

Using equation 19 we then obtain

$$Z_x(m) = -\frac{d_x}{\kappa_x^2} \int_{m\Delta t}^{(m+1)\Delta t} e^{-(d_x/\kappa_x + \alpha_x)\tau} d\tau = a_x e^{-(d_x/\kappa_x + \alpha_x) m\Delta t}, \quad (24)$$

with

$$b_x = e^{-(d_x/\kappa_x + \alpha_x)\Delta t}$$

and

$$a_x = \frac{d_x}{\kappa_x (d_x + \kappa_x \alpha_x)} (b_x - 1). \quad (25)$$

From a numerical point of view, the calculation of the convolution term written in equation 22 is costly because it requires at each time step a sum over all the previous time steps (sum over index m). Fortunately, as noted by Luebbers and Hunsberger (1992), because of the simple exponential form of term Z_x in equation 24, this sum can be efficiently performed based on a recursive convolution technique by considering ψ_x as a memory variable whose time evolution is governed at each time step by:

$$\psi_x^n = b_x \psi_x^{n-1} + a_x (\partial_x)^{n-1/2}. \quad (26)$$

This approach is interesting from a numerical point of view because it requires a computation time that is very small and because it implies the storage in memory of only one additional array for each derivative (and in the PML region only). To summarize, from a practical point of view, the implementation of the C-PML technique in an existing finite-difference code (without PML) is straightforward because one simply needs to replace each spatial derivative ∂_x with

$$\partial_{\tilde{x}} = \frac{1}{\kappa_x} \partial_x + \psi_x \quad (27)$$

and update ψ_x in time according to equation 26. The same approach can of course be used to implement C-PML layers along the other spatial directions (y or z). Let us note that, as in the classical PML, no particular treatment is needed in the corners of the grid: The ψ_x, ψ_y, and ψ_z contributions coming from the PML layers located along x, y, and z, respectively, are simply summed.

In terms of numerical efficiency, in Table 1 we give the maximum number of arrays that are needed in the PML layers to implement in 2D or 3D: the classical PML technique (e.g., Collino and Tsogka, 2001) without storing the total field, i.e., the sum of the split components, which is then recomputed in each loop; the classical PML technique, storing the total field; and the C-PML technique. This maximum number is reached in regions in which all the PML layers are present, i.e., in the corners of the domain. For comparison, we also recall the number of arrays needed when no absorbing conditions are implemented in the finite-difference technique. In the classical PML technique, the two options correspond to the fact that one can either choose to store the total field, which is needed several times in the algorithm at each time step, in addition to the split components of the field, which increases memory storage, but reduces computation time because one does not need to recompute the sum of the components several times in each iteration of the time loop. Or one can proceed the other way around and decide not to store the total field, but rather recompute it, which decreases memory storage, but increases CPU time. In any case, it is important to mention that the small difference in storage applies only in the PML layers and not in the main domain and is therefore negligible. For example, consider a typical 3D model of size $500 \times 500 \times 500$ grid points, with PML layers composed of 10 grid points on its six sides. The difference of three more arrays needed to implement C-PML, compared to PML without storing the total field, corresponds to $3 \times (500^3 - 480^3)$ stored values, compared to a total memory of 9×480^3 in the main domain without PML, plus $24 \times (500^3 - 480^3)$ in the PML layers, leads to an increase of only 3.2% of the total memory used.

NUMERICAL TESTS

To test the C-PML model introduced, we need to select a numerical method among all the widely used techniques mentioned in the introduction available to solve the differential seismic wave equation. We choose to implement the simplest technique, the finite-difference method, in which partial derivatives are approximated by discrete operators involving differences between adjacent grid

Table 1. Maximum number of arrays needed in the PML layers to implement in 2D or in 3D: the classical PML technique (e.g., Collino and Tsogka, 2001) without storing the total field, i.e. the sum of the split components, which is then recomputed in each loop; the classical PML technique, storing the total field; and the C-PML technique. This maximum number is reached in regions in which all the PML layers are present, i.e., in the corners of the domain. The small difference in storage applies only in the PML layers and not in the main domain and is therefore negligible. For comparison, we also recall the number of arrays needed when no absorbing conditions are implemented in the finite-difference technique.

	No PML	PML without total	PML with total	C-PML
2D	5	10	15	13
3D	9	24	33	27

points. More specifically, we use the classical second-order staggered grid in space and time used in many applications and introduced for Maxwell's equations by Yee (1966) and for elastodynamics by Madariaga (1976), and used by Virieux (1986).

Case of an isotropic medium

We consider a 3D model of size $1000 \times 6400 \times 6400$ m representing a domain much longer than wide (i.e., a thin slice) to favor the propagation of waves at grazing incidence, which constitutes the case, difficult for the classical PML technique, that we want to test. This model is discretized using a grid comprising 101 points $\times$ 641 points $\times$ 641 points. The size of a grid cell is $\Delta x = \Delta y = \Delta z = 10$ m. The nine variables v_x, v_y, v_z, σ_{xx}, σ_{yy}, σ_{zz}, σ_{xy}, σ_{xz}, and σ_{yz}, as well as the memory variables that implement the recursive convolution, are discretized on the grid represented in Figure 2. The medium is homogeneous and isotropic and has a compressional wave speed $c_p = 3300$ m.s^{-1}, a shear wave speed $c_s = c_p/\sqrt{3} \simeq 1905.3$ m.s^{-1} (i.e., Poisson's ratio is equal to 0.25), and density $\rho = 2800$ kg.m^{-3}. As time integration is based on an explicit scheme, the time step Δt must verify the Courant-Friedrichs-Lewy stability condition (Courant et al., 1928):

$$c_p \Delta t \sqrt{\frac{1}{\Delta x^2} + \frac{1}{\Delta y^2} + \frac{1}{\Delta z^2}} \leq 1. \qquad (28)$$

In the case of a uniform mesh size in all the spatial directions, i.e., when $\Delta x = \Delta y = \Delta z$ we thus have $c_p \Delta t / \Delta x \leq \sqrt{1/D}$, where D is the spatial dimension of the problem, i.e., in dimension $D = 3$ the upper bound is $1/\sqrt{3} \simeq 0.577$. We select $\Delta t = 1.6$ milliseconds, which corresponds to a Courant number of 0.528. We perform the simulation for 2500 time steps, i.e., a total duration of four seconds. Because the size of the mesh is large, we implement our finite-difference algorithm on a parallel computer based on a mixed message-passing MPI (e.g., Gropp et al., 1994) and shared-memory OpenMP (e.g., Chandra et al., 2000) model.

The point source is a velocity vector oriented at 135° in the (x,y) plane and located at $x = 790$ m, $y = 4270$ m, and $z = 3190$ m. Its time variation is the first derivative of a Gaussian of dominant frequency $f_0 = 7$ Hz shifted by $t_0 = 1.2/f_0 = 0.17$ second from time $t = 0$ to have null initial conditions. We record the time evolution of the components of the velocity vector at three points in the medium: ($x_1 = 200$ m, $y_1 = 4130$ m), ($x_2 = 700$ m, $y_2 = 2300$ m), and ($x_3 = 800$ m, $y_3 = 300$ m) in the same $z = 3190$ m plane as the source. The angle of 135° was selected for the source to have a radiation pattern that sends both significant P- and S-wave energy in the PML layers at both normal and grazing incidence.

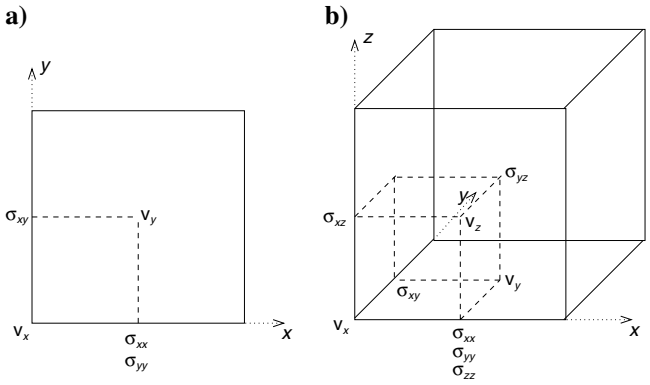

Figure 2. Elementary grid cells of the (a) 2D and (b) 3D staggered spatial finite-difference method of Madariaga (1976) and Virieux (1986) used classically to discretize the equations of elastodynamics.

Absorbing layers are implemented on the six sides of the model. They have a thickness of 100 m, which corresponds to 10 grid cells. Following Gedney (1998) and Collino and Tsogka (2001), for the damping coefficient in the PML we select a profile of the form $d_x(x) = d_0(x/L)^N$ along the x-axis, $d_y(y) = d_0(y/L)^N$ along the y-axis, and $d_z(z) = d_0(z/L)^N$ along the z-axis, where L is the thickness of the absorbing layer and $N = 2$. Recalling that the PML reflection coefficient is not exactly zero after discretization by any numerical scheme (e.g., Collino and Monk, 1998a), as mentioned in the introduction, we select a target theoretical reflection coefficient after discretization $R_c = 0.1\%$ and then define $d_0 = -(N+1)c_p \log(R_c)/(2L) \simeq 341.9$ as in Collino and Tsogka (2001). Following Roden and Gedney (2000), we choose to make α_x, α_y, and α_z vary in a linear fashion in their respective PML layer between a maximum value $\alpha_{\max}$ at the beginning (i.e., the entrance) of the PML and zero at its top. As in Festa and Vilotte (2005), we take $\alpha_{\max} = \pi f_0$, where f_0 is the dominant frequency of the source defined above. Variable κ was introduced in Roden and Gedney (2000) primarily to attenuate evanescent waves in electromagnetics. Several numerical tests (not presented here) indicate that in the case of the seismic wave equation it does not seem to have a crucial effect, and we therefore choose $\kappa_x = \kappa_y = \kappa_z = 1$. On the external edges of the layer at the top of the PML, we impose a Dirichlet condition on the velocity vector ($\mathbf{v} = \mathbf{0}$ for all t). Let us note that it is crucial to correctly define coefficients a_x, b_x, a_y, b_y, a_z, and b_z that govern the time evolution of the memory variables (equation 25) at the right location in the staggered grid of Figure 2. Coefficients a_x and b_x must be defined at the grid cell for memory variables ψ_x acting on v_x, σ_{xy}, and σ_{xz}, but at half the grid cell for those acting on v_y, v_z, σ_{xx}, σ_{yy}, σ_{zz}, and σ_{yz}. Similarly, a_y and b_y must be defined at the grid cell for memory variables ψ_y acting on v_x, v_z, σ_{xx}, σ_{yy}, σ_{zz}, and σ_{xz}, but at half the grid cell for those acting on v_y, σ_{xy}, and σ_{yz}. In the same fashion, a_z and b_z must be defined at the grid cell for memory variables ψ_z acting on v_x, v_y, σ_{xx}, σ_{yy}, σ_{zz}, and σ_{xy}, but at half the grid cell for those acting on v_z, σ_{xz}, and σ_{yz}. Let us also note that, as in the classical PML formulation, in the corners of the grid the contributions coming from the terms in which d_x, d_y, or d_z appear are simply summed. The corners are thus treated naturally without any modification of the computer code.

Figure 3 represents snapshots of the v_y component of the velocity vector in the (x,y) plane located at $z = 3190$ m at six different time steps for a simulation with C-PML. No spurious waves of significant amplitude are visible, even at grazing incidence. It is important to compare the behavior of the C-PML condition at grazing incidence to that of the classical PML model (e.g., Collino and Tsogka, 2001) implemented based on split fields. Figure 4 represents the same snapshots when the classical PML is implemented. One can notice that spurious waves appear at grazing incidence along the edges of the model and send spurious energy back into the main domain. Figure 5 represents the time evolution at the three recording points of the v_x and v_y components of the velocity vector for the numerical calculations with C-PML compared with the exact solution of the problem. Let us mention that the exact solution of the numerical problem is purposely computed numerically (rather than analytically) using the same finite-difference method without C-PML on a very large mesh to have exactly the same numerical dispersion in the reference

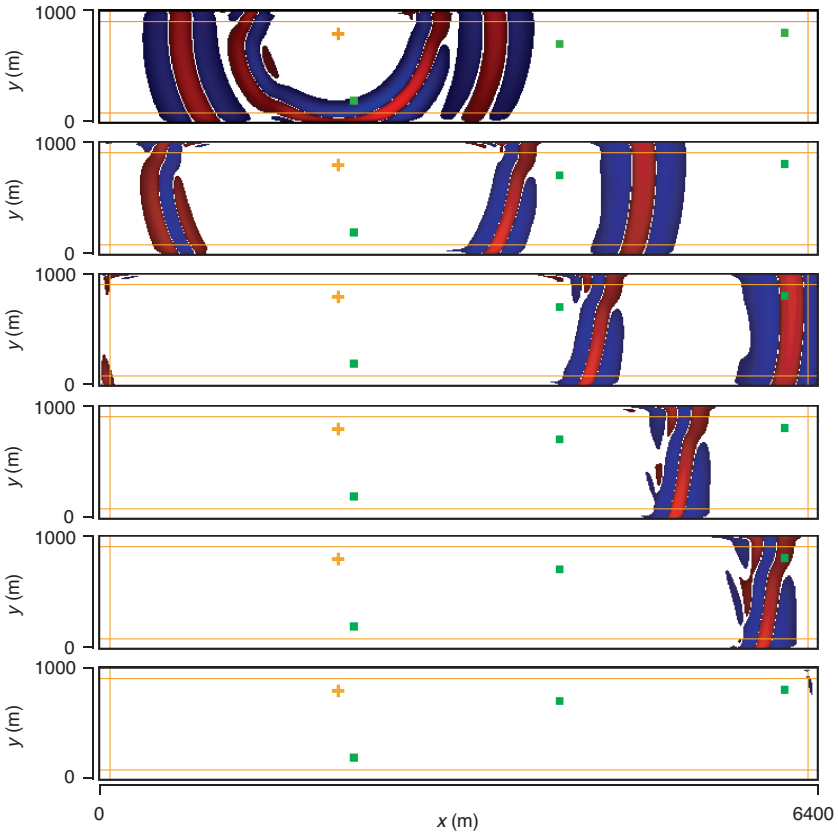

Figure 3. Snapshots in the (x,y) plane located at z = 3190 m of the v_y component of the 3D velocity vector for a model corresponding to a thin slice with C-PML conditions implemented on the six sides, at time 0.6 s (top), 1 s, 1.4 s, 1.8 s, 2.2 s, and 2.6 s (bottom). We represent the component in red (positive) or blue (negative) at each grid point when it has an amplitude higher than a threshold of 1% of the maximum, and the normalized value is raised to the power 0.30 to enhance small amplitudes that would otherwise not be clearly visible. The orange cross indicates the position of the source and the green squares indicate the position of the receivers at which the seismograms represented in Figure 5 are recorded. The four vertical or horizontal orange lines represent the edge of each layer PML. No spurious wave of significant amplitude is visible, even at grazing incidence. The snapshots have been rotated by 90° to fit on the page.

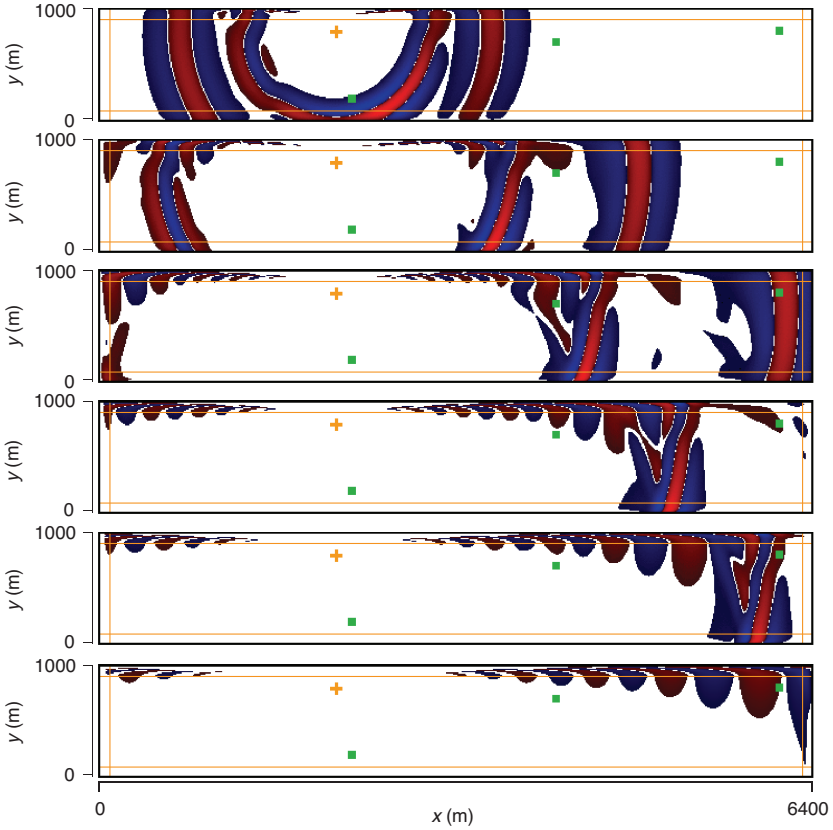

Figure 4. Snapshots in the (x,y) plane located at z = 3190 m of the v_y component of the 3D velocity vector for a model corresponding to a thin slice with classical PML conditions (e.g., Collino and Tsogka, 2001) implemented on the six sides, at time 0.6 s (top), 1 s, 1.4 s, 1.8 s, 2.2 s, and 2.6 s (bottom). We represent the component in red (positive) or blue (negative) at each grid point when it has an amplitude higher than a threshold of 1% of the maximum, and the normalized value is raised to the power 0.30 to enhance small amplitudes that would otherwise not be clearly visible. The orange cross indicates the position of the source and the green squares indicate the position of the receivers at which the seismograms represented in Figure 6 are recorded. The four vertical or horizontal orange lines represent the edge of each layer PML. Compared to Figure 3, spurious waves appear at grazing incidence along the edges of the model and send spurious energy back into the main domain. The snapshots have been rotated by 90° to fit on the page.

solution and be able to focus on artifacts coming from the C-PML edges only. Strictly speaking it is therefore very accurate, but not exact. At the first receiver, relatively far from the beginning (i.e., the entrance) of the PML layer and at nongrazing incidence, the agreement is almost perfect. At the second receiver, at grazing incidence and rather close to the beginning of the PML layer, the agreement remains good. At the third receiver, in the difficult case of very grazing incidence, of a long distance of propagation, thus accumulating numerical dispersion, and of a receiver located close to the beginning of the PML layer (at a distance of 100 m, which corresponds to 10 grid cells), the agreement remains satisfactory, which illustrates the good performance of the C-PML. To compare again the behavior of the C-PML condition at grazing incidence to that of the classical PML model (e.g., Collino and Tsogka, 2001) implemented based on split fields, Figure 6 represents the same test when the classical PML model is used. At the first receiver, close to normal incidence, both C-PML and PML give an almost perfect result. But at the second receiver, spurious oscillations start to appear in the case of PML, which can be observed in particular for the S-wave on the v_y component. At the third receiver, the oscillations become large, the P-wave is not correctly calculated and the shape of the S-wave is completely distorted. Overall, it is clear that the results given by the classical PML model exhibit more oscillations and of larger amplitude than the C-PML solution, which illustrates the efficiency of the C-PML condition at grazing incidence.

We now study the decay of energy in the grid to check the efficiency of the discrete C-PML model, in particular at grazing incidence. Figure 7 represents the time decay of total energy:

$$E = \frac{1}{2}\rho\|\mathbf{v}\|^2 + \frac{1}{2}\sum_{i=1}^{D}\sum_{j=1}^{D}\sigma_{ij}\varepsilon_{ij} \tag{29}$$

in the main domain (i.e., in the medium without the six PML layers) for the simulation presented in Figure 3 for C-PML and in Figure 4 for PML. We observe that between approximately 0 and 0.25 s, the source injects energy in the medium. Then, the energy carried by the P- and S-waves is gradually absorbed in the PML layers. Around approximately 3 s the S-wave, which is slower, reaches the farthest edge of the grid and should then theoretically completely leave the medium, which results in a steep decay of total energy. After approximately 3 s, theoretically there should remain no energy in the medium because both the P- and S-waves have left the main domain. All the energy that remains is therefore spurious and constitutes a good measurement of the efficiency of the absorbing technique used. In the case of PML, at 4 s there remains a total energy of 235.12 J, whereas in the case of C-PML there remains a total of 3.83×10^{-2} J, i.e., 6139 times smaller.

It is also interesting to study the issue of the stability of the C-PML model at longer times. Indeed, we know that in many PML models, for example in the case of Maxwell's equations, weak or strong instabilities can develop at longer times (e.g., Abarbanel et al., 2002; Bécache and Joly, 2002; Bécache et al., 2004). To study this question from a numerical point of view, in Figure 8 we make the experiment of Figure 3 last for 100,000 time steps instead of 2500. Total energy decreases continuously and we do not observe instabilities developing, which means that the discrete C-PML model is stable up to 160 s.

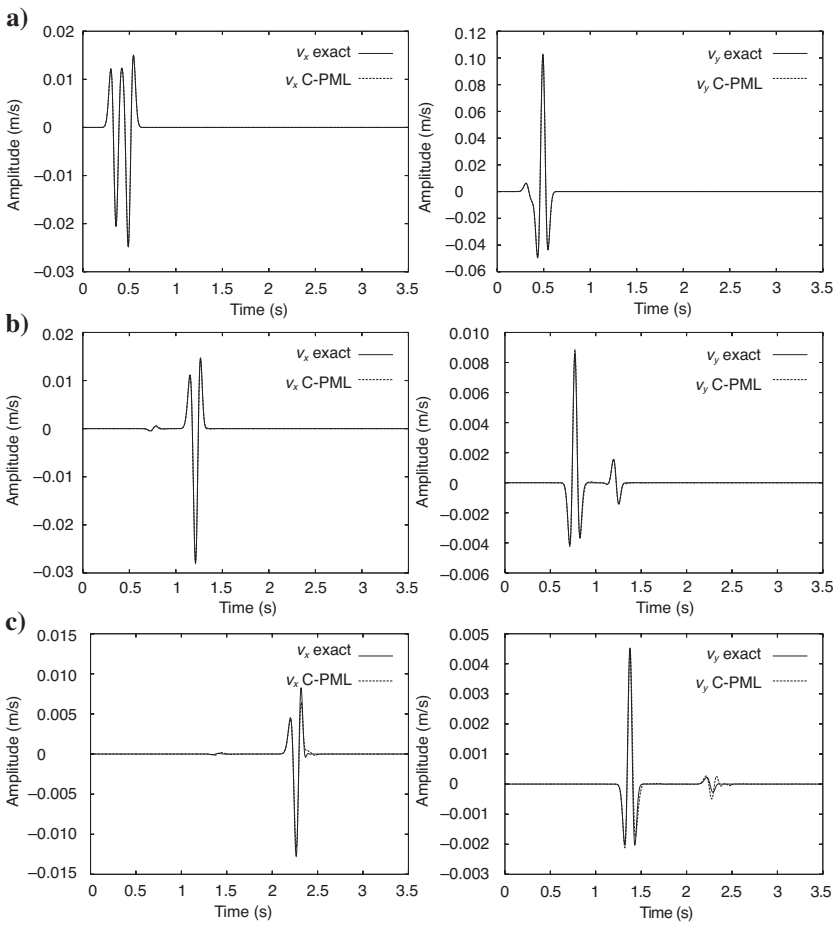

Figure 5. Time evolution of the v_x (left) and v_y (right) components of the 3D velocity vector at the (a) first, (b) second, and (c) third receiver of the exact solution of the problem (solid line) and the numerical solution with C-PML (dotted line) for the numerical experiment of Figure 3. At the first receiver, relatively far from the beginning (i.e. the entrance) of the PML layer and with nongrazing incidence, the agreement is almost perfect. At the second receiver, with grazing incidence and rather close to the beginning of the PML layer, the agreement remains good. At the third receiver, in the difficult case of very grazing incidence, of a long distance of propagation, thus accumulating numerical dispersion, and of a receiver located close to the beginning of the PML layer (at a distance of 100 m, which corresponds to 10 grid cells), the agreement remains satisfactory, which illustrates the good performance of the C-PML.

Case of an anisotropic medium

We have seen above that the C-PML technique consists of replacing spatial derivatives in the seismic wave equation 7 with the modified equation 27, in which the time evolution of the memory variable ψ_x is governed by equation 26, with coefficients a_x and b_x given by equation 25 that do not depend on the physical properties of the medium. Therefore, the method should work in the anisotropic case without any modification.

To validate it in such a case, we study two orthotropic crystals, previously analyzed by Bécache et al. (2003) and whose slowness curves are given there, in the ultrasonic frequency range. For comparison we perform the simulations in two dimensions, as in Bécache et al. (2003). The five variables v_x, v_y, σ_{xx}, σ_{yy}, and σ_{xy}, as well as the memory variables that implement the recursive convolution, are discretized on the grid represented in Figure 2. For the first medium, the anisotropic constants are $c_{11} = 4\times10^{10}$ N.m^{-2}, $c_{22} = 20\times10^{10}$ N.m^{-2}, $c_{12} = 3.8\times10^{10}$ N.m^{-2}, $c_{33} = 2\times10^{10}$ N.m^{-2}, and $\rho = 4000$ kg.m^{-3}, and for the second medium they are $c_{11} = c_{22} = 20\times10^{10}$ N.m^{-2}, $c_{12} = 3.8\times10^{10}$ N.m^{-2}, $c_{33} = 2\times10^{10}$ N.m^{-2}, and $\rho = 4000$ kg.m^{-3}. The size of the model is 25×25 cm. The source is a vertical force located at the center of the model and with a dominant frequency f_0 of 200 kHz, shifted by $t_0 = 7$ μs from time $t = 0$ to have null initial conditions. The mesh is composed of 401×401 grid points, i.e., the size of a grid cell is 0.0625 cm, and the time step is 50 nanoseconds, because in dimension $D = 2$ the upper bound of the Courant stability condition is $1/\sqrt{2}\simeq0.707$. The simulation is performed for a total duration of 150 μs. The PML regions have a thickness of 0.625 cm, which corresponds to 10 grid cells, and are implemented on the four sides of the mesh to mimic an infinite medium. We use the same scaling as in the isotropic case above for the damping coefficients. Figure 9 shows snapshots of wave propagation at times $t = 20$ μs, $t = 40$ μs, $t = 60$ μs, and $t = 80$ μs. One can observe that the classical patterns in such anisotropic media, namely the quasi-pressure (qP) wave and the quasi-shear (qS) wave, are efficiently absorbed and that no numerical instabilities appear. We then let the simulation run for 20,000 time steps to check the stability of the method from an experimental point of view and did not observe any instability.

Unfortunately, Bécache et al. (2003) have shown that the stability of the classical PML model depends on the physical properties of the anisotropic medium and that the model can be intrinsically unstable (mathematically, before numerical discretization) for some anisotropic media, for instance if the stiffness parameters do not satisfy the following three necessary high-frequency stability conditions:

$$\begin{aligned}((c_{12}+c_{33})^2 - c_{11}(c_{22}-c_{33}))((c_{12}+c_{33})^2 \\ + c_{33}(c_{22}-c_{33})) \le 0,\\ (c_{12}+2c_{33})^2 - c_{11}c_{22} \le 0,\\ (c_{12}+c_{33})^2 - c_{11}c_{22} - c_{33}^2 \le 0. \quad (30)\end{aligned}$$

These conditions can be interpreted in terms of the geometric properties of the slowness surfaces: For instance, a PML parallel to the x-axis (thus absorbing waves coming from the $y\le0$ half-space) is unstable if projections of the slowness vector and of the group velocity vector on the y-axis have opposite signs. The geometric condition is satisfied for all the slowness curves related to the qP-waves, and therefore the cause of the instabilities reported by Bécache et al. (2003) comes from the violation of the high-frequency stability condition by the qS-waves. Because we have not changed the basic mathematical idea behind the PML (we have simply used the more general complex coordinate transform of equation 15 instead of equation 5), the C-PML model suffers from the same limitation and is intrinsically unstable if the anisotropic medium does not satisfy the stability conditions of equation 30.

To illustrate this, we study two transversely isotropic crystals with a vertical symmetry axis, apatite and zinc, in the ultrasonic frequency range (e.g., Komatitsch et al., 2000). For apatite, the anisotropic constants are $c_{11} = 16.7\times10^{10}$ N.m^{-2}, $c_{22} = 14\times10^{10}$ N.m^{-2}, $c_{12} = 6.6\times10^{10}$ N.m^{-2}, $c_{33} = 6.63\times10^{10}$ N.m^{-2}, and $\rho = 3200$ kg.m^{-3}, and for zinc, they are $c_{11} = 16.5\times10^{10}$ N.m^{-2}, $c_{22} = 6.2\times10^{10}$ N.m^{-2}, $c_{12} = 5\times10^{10}$ N.m^{-2}, $c_{33} = 3.96\times10^{10}$ N.m^{-2}, and $\rho = 7100$ kg.m^{-3}. The source now has a dominant frequency of 300 kHz for apatite and of 170 kHz for zinc. Figure 10 shows that strong instabilities develop in the PML when the slowest wave, i.e., the qS-wave with its cuspidal triangles, penetrates in the layer and that the simulation becomes unstable.

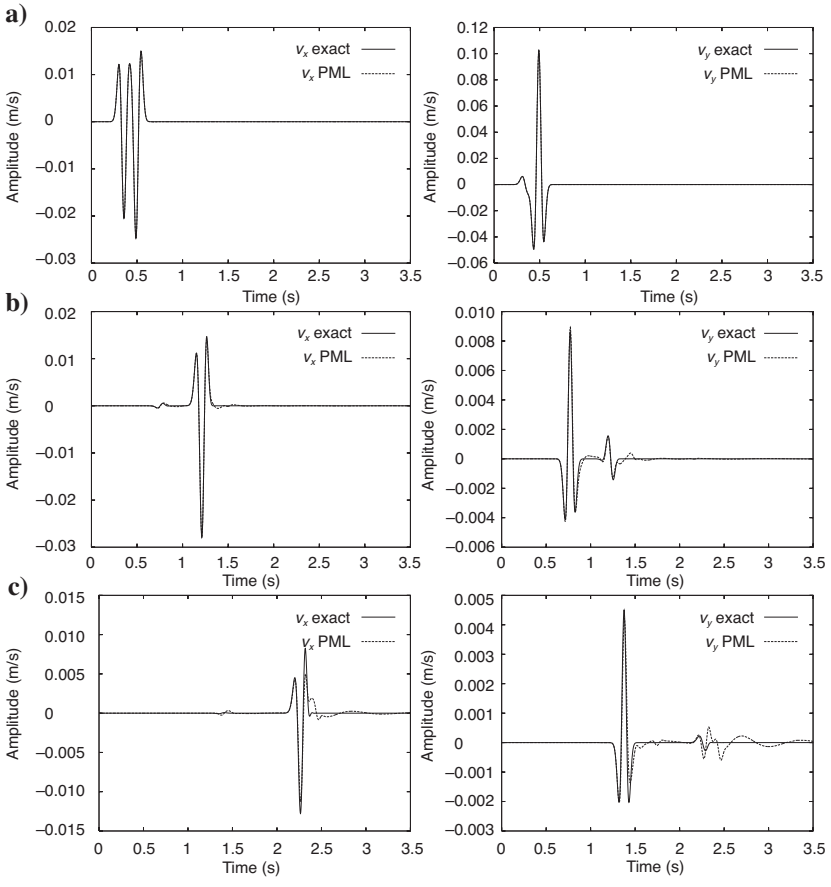

Figure 6. Time evolution of the v_x (left) and v_y (right) components of the 3D velocity vector at the (a) first, (b) second, and (c) third receiver of the exact solution of the problem (solid line) and the numerical solution with the classical PML (e.g., Collino and Tsogka, 2001) (dotted line) for the numerical experiment of Figure 4. At the first receiver, relatively far from the beginning (i.e. the entrance) of the PML layer and with nongrazing incidence, the agreement is almost perfect. But compared to Figure 5, at the second receiver spurious oscillations, which can be observed in particular for the S-wave on the v_y component, start to appear. At the third receiver, the oscillations become large, the P-wave is not correctly calculated and the shape of the S-wave is completely distorted.

It is important to note that the model is unstable for rather common materials (such as zinc) and, therefore, it is not very useful in practice for crystals because many widely studied anisotropic media will violate the stability conditions (equation 30). A somewhat similar situation (although simpler, because the slowness curves of crystals can be very complex) is found in aeroacoustics, for which the classical PML model must be reformulated to be made stable (Abarbanel et al., 1999; Hu, 2001; Diaz and Joly, 2006). It would be interesting to study if a similar approach could be used to stabilize PML in anisotropic media. Let us also mention that some slowly growing instabilities might not be observed if one uses a relatively small number of time steps, as for the anisotropic simulations in Collino and Tsogka (2001), but that they become clear if one lets the simulation run for a sufficiently large number of time steps.

It is equally important to mention that the situation is very different in other fields, such as the simulation of seismic wave propagation in the oil industry or in global or regional seismology, in which anisotropy always consists in small perturbations of a few percents with respect to an isotropic reference model, in which case the stability conditions (equation 30) will always be fulfilled.

In terms of the intrinsic instabilities observed for some anisotropic materials (Bécache et al., 2003; Appelö and Kreiss, 2006), in future work it would be interesting to try to overcome such limitations based on the modal approach of Hagstrom (2003) and Appelö and Kreiss (2006), on new models such as that of Rahmouni (2004), or on ideas similar to that used to make the PML stable in aeroacoustics (Abarbanel et al., 1999; Hu, 2001; Diaz and Joly, 2006).

A future development could be to replace the Dirichlet boundary conditions implemented at the top of the PML with a paraxial absorbing boundary condition to further improve the numerical efficiency of the discrete PML, as done in the case of Maxwell's equations for instance by Collino and Monk (1998a) and Fontes (2006), who used a Silver-Müller condition instead of a Dirichlet condition.

The source code of our finite-difference program SEISMIC_CPML is freely available under CeCILL license (a French equivalent of GNU GPL) from www.univ-pau.fr/~dkomati1.

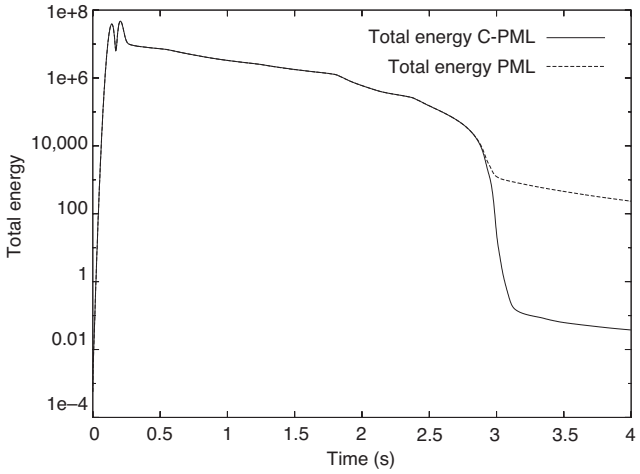

Figure 7. Decay of total energy with time in the main domain (i.e., in the medium without the six PML layers) on a semilogarithmic scale for the simulations presented in Figures 3 and 4. One can observe that between approximately 0 and 0.25 s, the source injects energy in the medium. Then, the energy carried by the P- and S-waves is gradually absorbed in the PML layers. Around approximately 3 s the S-wave, which is slower, reaches the farthest edge of the grid and should then theoretically completely leave the medium, which results in a steep decay of total energy. After approximately 3 s, theoretically there should remain no energy in the medium because both the P- and S-waves have left the main domain. All the energy that remains is therefore spurious and constitutes a good measurement of the efficiency of the absorbing technique used. In the case of PML, at 4 s there remains a total energy of 235.12 J, whereas in the case of C-PML there remains a total of 3.83×10^{-2} J, i.e., 6139 times smaller. This illustrates the efficiency of the C-PML technique, including at grazing incidence.

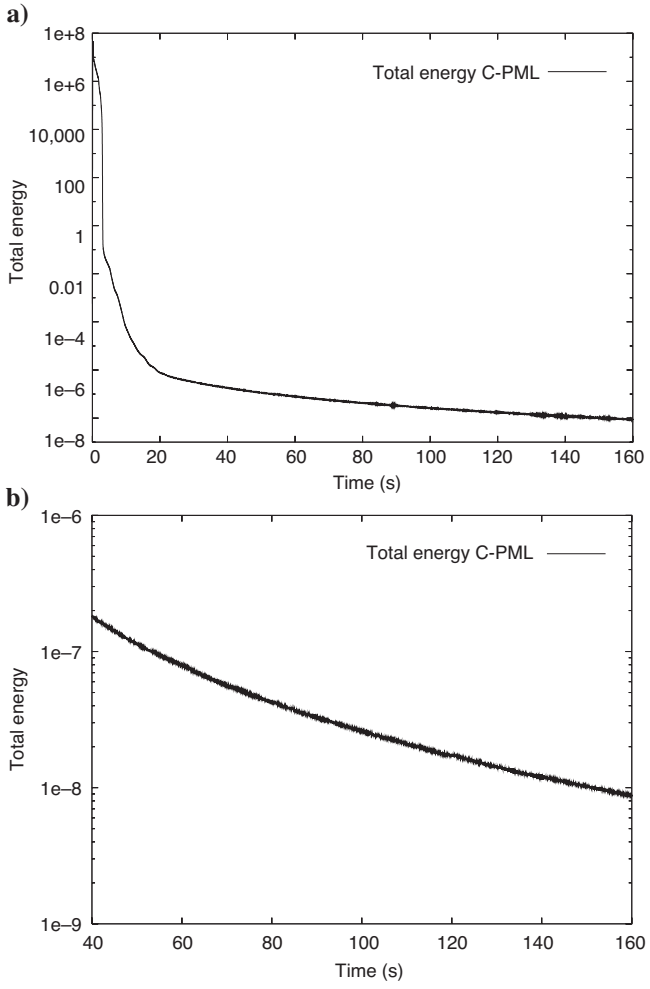

Figure 8. To study the stability of the C-PML model at longer times, we make the experiment of Figures 3 and 7 last for 100,000 time steps instead of 2500. Total energy decreases continuously and we do not observe instabilities developing on this semilogarithmic plot (a), which means that the discrete C-PML model is stable up to 160 s. By looking at a close-up on the second part of the curve (b), approximately between times $t = 80$ s and $t = 160$ s one can notice tiny oscillations that are because of the fact that total energy is so small that we start to see the effect of roundoff of floating-point numbers of the computer.

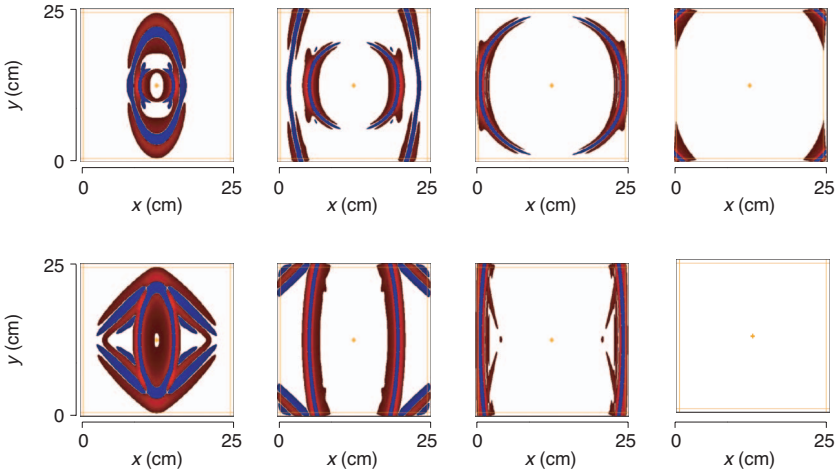

Figure 9. Snapshots at time $t = 20$ μs, $t = 40$ μs, $t = 60$ μs, and $t = 80$ μs (from left to right) of the vertical component of the 2D velocity vector for two anisotropic crystals (top and bottom) with C-PML conditions implemented on the four edges of the grid to mimic an infinite medium. We represent the component in red (positive) or blue (negative) at each grid point when it has an amplitude higher than a threshold of 1% of the maximum, and the normalized value is raised to the power 0.30 to enhance small amplitudes that would otherwise not be clearly visible. The orange cross indicates the position of the vertical force source and the four orange vertical and horizontal lines represent the boundary of each PML. One can observe that the classical patterns in such anisotropic crystals, namely the quasi-pressure (qP) wave and the quasi-shear (qS) wave, are efficiently absorbed because no significant spurious waves are reflected off the boundaries, and that no numerical instabilities appear.

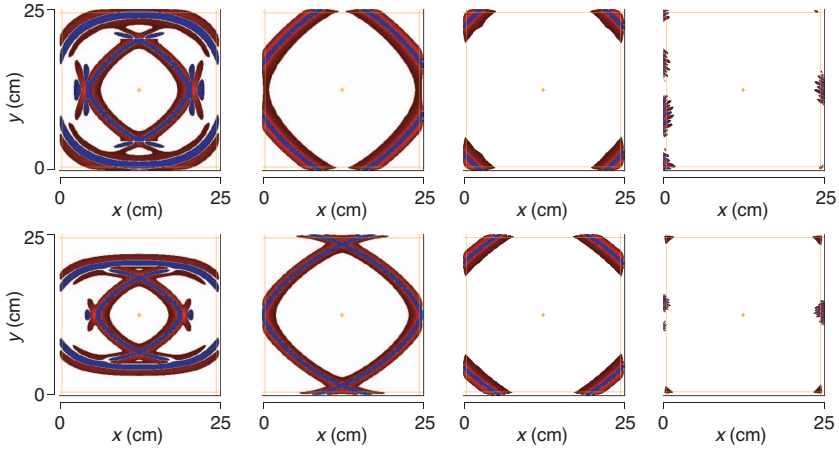

Figure 10. Snapshots in the case of two anisotropic materials for which the PML model is intrinsically unstable mathematically before discretization (Bécache et al., 2003): a crystal of apatite (top) and zinc (bottom) with C-PML conditions implemented on the four edges of the grid to mimic an infinite medium. The vertical component of the 2D velocity vector is represented at time $t = 25$ μs, $t = 40$ μs, $t = 50$ μs, and $t = 140$ μs from left to right for apatite and at time $t = 35$ μs, $t = 60$ μs, $t = 85$ μs, and $t = 125$ μs from left to right for zinc. We represent the component in red (positive) or blue (negative) at each grid point when it has an amplitude higher than a threshold of 1% of the maximum, and the normalized value is raised to the power 0.30 to enhance small amplitudes that would otherwise not be clearly visible. The orange cross indicates the position of the vertical force source and the four orange vertical and horizontal lines represent the boundary of each PML. Strong instabilities develop in the PML when the slowest wave, i.e. the qS-wave with its cuspidal triangles, penetrates in the layer, and the simulation becomes unstable (right).

CONCLUSIONS

We improved the behavior of the PML at grazing incidence for the differential seismic wave equation based on an unsplit convolutional approach. This improved PML can be useful, for instance, in the case of thin mesh slices, in the case of sources located close to the edge of the mesh, and/or in the case of receivers located at very large offset, i.e., rather common situations that are of interest for instance for oil industry simulations. The cost of the improved PML in terms of memory storage is similar to that of the classical PML.

We demonstrated the efficiency of this improved C-PML based on numerical benchmarks using a finite-difference method on a thin mesh slice for an isotropic material. We showed that results are significantly improved compared with the classical PML technique.

We did not change the basic idea behind the PML and, therefore, found the same limitations as with the classical PML for some anisotropic materials for which the mathematical PML model has intrinsic instabilities before discretization.

ACKNOWLEDGMENTS

The authors would like to thank Stephen D. Gedney for fruitful discussions and for providing them with his C-PML software package for Maxwell's equations, Hélène Barucq and Mathieu Fontes for discussions about the inverse Fourier and Laplace transforms of the operators used, and Julien Diaz for discussions about the stability of PML in aeroacoustics. The comments and suggestions of Yong-Hua Chen, four anonymous reviewers, the assistant and associate editor, and editor Yonghe Sun helped to improve the manuscript. Calculations were performed on an IBM Power4 at Institut du Développement et des Ressources en Informatique Scientifique under project 072102 and on the Division of Geological & Planetary Sciences Dell cluster at the California Institute of Technology. This material is based in part upon research supported by European FP6 Marie Curie International Reintegration Grant MIRG-CT-2005-017461. It was presented at the 2005 Fall Meeting of the American Geophysical Union (Martin et al., 2005) and at the 2006 General Assembly of the European Geosciences Union (Martin and Komatitsch, 2006).

REFERENCES

Abarbanel, S., D. Gottlieb, and J. S. Hesthaven, 1999, Well-posed perfectly matched layers for advective acoustics: Journal of Computational Physics, **154**, 266–283.

———, 2002, Long-time behavior of the perfectly matched layer equations in computational electromagnetics: Journal of Scientific Computing, **17**, 405–422.

Alterman, Z., and F. C. Karal, 1968, Propagation of elastic waves in layered media by finite difference methods: Bulletin of the Seismological Society of America, **58**, 367–398.

Appelö, D., and G. Kreiss, 2006, A new absorbing layer for elastic waves: Journal of Computational Physics, **215**, 642–660.

Bao, H., J. Bielak, O. Ghattas, L. F. Kallivokas, D. R. O'Hallaron, J. R. Shew-

chuk, and J. Xu, 1998, Large-scale simulation of elastic wave propagation in heterogeneous media on parallel computers: Computer Methods in Applied Mechanics and Engineering, **152**, 85–102.
Basu, U., and A. K. Chopra, 2004, Perfectly matched layers for transient elastodynamics of unbounded domains: International Journal for Numerical Methods in Engineering, **59**, 1039–1074.
Bécache, E., S. Fauqueux, and P. Joly, 2003, Stability of perfectly matched layers, group velocities and anisotropic waves: Journal of Computational Physics, **188**, 399–433.
Bécache, E., and P. Joly, 2002, On the analysis of Bérenger's perfectly matched layers for Maxwell's equations: Mathematical Modelling and Numerical Analysis, **36**, 87–120.
Bécache, E., P. G. Petropoulos, and S. G. Gedney, 2004, On the long-time behavior of unsplit perfectly matched layers: IEEE Transactions on Antennas and Propagation, **52**, 1335–1342.
Bérenger, J. P., 1994, A perfectly matched layer for the absorption of electromagnetic waves: Journal of Computational Physics, **114**, 185–200.
———, 1996, Three-dimensional perfectly matched layer for the absorption of electromagnetic waves: Journal of Computational Physics, **127**, 363–379.
———, 2002a, Application of the CFS PML to the absorption of evanescent waves in waveguides: IEEE Microwave and Wireless Components Letters, **12**, 218–220.
———, 2002b, Numerical reflection from FDTD-PMLs: A comparison of the split PML with the unsplit and CFS PMLs: IEEE Transactions on Antennas and Propagation, **50**, 258–265.
Bermúdez, A., L. Hervella-Nieto, A. Prieto, and R. Rodríguez, 2007, An optimal perfectly matched layer with unbounded absorbing function for time-harmonic acoustic scattering problems: Journal of Computational Physics, **223**, 469–488.
Carcione, J. M., 1994, The wave equation in generalized coordinates: Geophysics, **59**, 1911–1919.
Carcione, J. M., D. Kosloff, and R. Kosloff, 1988, Wave propagation simulation in a linear viscoelastic medium: Geophysical Journal International, **95**, 597–611.
Cerjan, C., D. Kosloff, R. Kosloff, and M. Reshef, 1985, A nonreflecting boundary condition for discrete acoustic and elastic wave equation: Geophysics, **50**, 705–708.
Chaljub, E., Y. Capdeville, and J. P. Vilotte, 2003, Solving elastodynamics in a fluid-solid heterogeneous sphere: A parallel spectral element approximation on non-conforming grids: Journal of Computational Physics, **187**, 457–491.
Chandra, R., R. Menon, L. Dagum, D. Kohr, D. Maydan, and J. McDonald, 2000, Parallel programming in OpenMP: Morgan Kaufmann.
Chew, W. C., and Q. Liu, 1996, Perfectly matched layers for elastodynamics: A new absorbing boundary condition: Journal of Computational Acoustics, **4**, 341–359.
Chew, W. C., and W. H. Weedon, 1994, A 3-D perfectly matched medium from modified Maxwell's equations with stretched coordinates: Microwave and Optical Technology Letters, **7**, 599–604.
Clayton, R., and B. Engquist, 1977, Absorbing boundary conditions for acoustic and elastic wave equations: Bulletin of the Seismological Society of America, **67**, 1529–1540.
Cohen, G., and S. Fauqueux, 2005, Mixed spectral finite elements for the linear elasticity system in unbounded domains: SIAM Journal on Scientific Computing, **26**, 864–884.
Cohen, G., P. Joly, and N. Tordjman, 1993, Construction and analysis of higher-order finite elements with mass lumping for the wave equation: Proceedings of the 2nd International Conference on Mathematical and Numerical Aspects of Wave Propagation, SIAM, 152–160.
Collino, F., and P. Monk, 1998a, Optimizing the perfectly matched layer: Computer Methods in Applied Mechanics and Engineering, **164**, 157–171.
———, 1998b, The perfectly matched layer in curvilinear coordinates: SIAM Journal on Scientific Computing, **19**, 2061–2090.
Collino, F., and C. Tsogka, 2001, Application of the PML absorbing layer model to the linear elastodynamic problem in anisotropic heterogeneous media: Geophysics, **66**, 294–307.
Courant, R., K. O. Friedrichs, and H. Lewy, 1928, Über die partiellen Differenzengleichungen der mathematischen Physik: Mathematische Annalen, **100**, 32–74.
Day, S. M., 1998, Efficient simulation of constant Q using coarse-grained memory variables: Bulletin of the Seismological Society of America, **88**, 1051–1062.
Diaz, J., and P. Joly, 2006, A time-domain analysis of PML models in acoustics: Computer Methods in Applied Mechanics and Engineering, **195**, 3820–3853.
Dong, L., D. She, L. Guan, and Z. Ma, 2005, An eigenvalue decomposition method to construct absorbing boundary conditions for acoustic and elastic wave equations: Journal of Geophysics and Engineering, **2**, 192–198.
Drossaert, F. H., and A. Giannopoulos, 2007a, Complex frequency shifted convolution PML for FDTD modelling of elastic waves: Wave Motion, **44**, 593–604, http://dx.doi.org/10.1016/j.wavemoti.2007.03.003.
———, 2007b, A nonsplit complex frequency-shifted PML based on recursive integration for FDTD modeling of elastic waves: Geophysics, **72**, no. 2, T9–T17.
Dumbser, M., and M. Käser, 2006, An arbitrary high-order discontinuous Galerkin method for elastic waves on unstructured meshes-II. The three-dimensional isotropic case: Geophysical Journal International, **167**, 319–336.
Engquist, B., and A. Majda, 1977, Absorbing boundary conditions for the numerical simulation of waves: Mathematical Computing, **31**, 629–651.
Faccioli, E., F. Maggio, R. Paolucci, and A. Quarteroni, 1997, 2D and 3D elastic wave propagation by a pseudo-spectral domain decomposition method: Journal of Seismology, **1**, 237–251.
Festa, G., E. Delavaud, and J. P. Vilotte, 2005, Interaction between surface waves and absorbing boundaries for wave propagation in geological basins: 2D numerical simulations: Geophysical Research Letters, **32**, L20306.
Festa, G., and S. Nielsen, 2003, PML absorbing boundaries: Bulletin of the Seismological Society of America, **93**, 891–903.
Festa, G., and J. P. Vilotte, 2005, The Newmark scheme as velocity-stress time-staggering: An efficient PML implementation for spectral-element simulations of elastodynamics: Geophysical Journal International, **161**, 789–812.
Fontes, M., 2006, Propriétés mathématiques de modèles géophysiques pour l'absorption des ondes. Application aux conditions de bords absorbants: Ph.D. thesis, Université de Pau et des Pays de l'Adour.
Gedney, S. D., 1996, An anisotropic perfectly matched layer-absorbing medium for the truncation of FDTD lattices: IEEE Transactions on Antennas and Propagation, **44**, 1630–1639.
———, 1998, The perfectly matched layer absorbing medium, *in* A. Taflove, ed., Advances in computational electrodynamics: The finite-difference time-domain method: Artech House Antenna Library, 263–343.
Givoli, D., 1991, Non-reflecting boundary conditions: Review article: Journal of Computational Physics, **94**, 1–29.
Gropp, W., E. Lusk, and A. Skjellum, 1994, Using MPI, portable parallel programming with the message-passing interface: MIT Press.
Grote, M. J., 2000, Nonreflecting boundary conditions for elastodynamics scattering: Journal of Computational Physics, **161**, 331–353.
Guddati, M. N., and K. W. Lim, 2006, Continued fraction absorbing boundary conditions for convex polygonal domains: International Journal for Numerical Methods in Engineering, **66**, 949–977.
Hagstrom, T., 2003, A new construction of perfectly matched layers for hyperbolic systems with applications to the linearized Euler equations *in* G. C. Cohen, E. Heikkola, P. Joly, and P. Neittaanmaki, eds., Mathematical and numerical aspects of wave propagation: Waves 2003, Springer-Verlag 125–129.
Hagstrom, T., and S. I. Hariharan, 1998, A formulation of asymptotic and exact boundary conditions using local operators: Applied Numerical Mathematics, **27**, 403–416.
Hastings, F. D., J. B. Schneider, and S. L. Broschat, 1996, Application of the perfectly matched layer (PML) absorbing boundary condition to elastic wave propagation: Journal of the Acoustical Society of America, **100**, 3061–3069.
Hesthaven, J. S., 1998, On the analysis and construction of perfectly matched layers for the linearized Euler equations: Journal of Computational Physics, **142**, 129–147.
Higdon, R. L., 1991, Absorbing boundary conditions for elastic waves: Geophysics, **56**, 231–241.
Hu, F. Q., 2001, A stable perfectly matched layer for linearized Euler equations in unsplit physical variables: Journal of Computational Physics, **173**, 455–480.
Katsibas, T. K., and C. S. Antonopoulos, 2002, An efficient PML absorbing medium in FDTD simulations of acoustic scattering in lossy media: IEEE Proceeding on Ultrasonic Symposium, 551–554.
Kawase, H., 1988, Time-domain response of a semi-circular canyon for incident *SV*, *P* and Rayleigh waves calculated by the discrete wavenumber boundary element method: Bulletin of the Seismological Society of America, **78**, 1415–1437.
Komatitsch, D., C. Barnes, and J. Tromp, 2000, Simulation of anisotropic wave propagation based upon a spectral element method: Geophysics, **65**, 1251–1260.
Komatitsch, D., and J. Tromp, 1999, Introduction to the spectral-element method for 3-D seismic wave propagation: Geophysical Journal International, **139**, 806–822.
———, 2003, A perfectly matched layer absorbing boundary condition for the second-order seismic wave equation: Geophysical Journal International, **154**, 146–153.
Komatitsch, D., and J. P. Vilotte, 1998, The spectral-element method: An efficient tool to simulate the seismic response of 2D and 3D geological structures: Bulletin of the Seismological Society of America, **88**, 368–392.
Kosmanis, T. I., T. V. Yioultsis, and T. D. Tsiboukis, 1999, Perfectly matched anisotropic layer for the numerical analysis of unbounded eddy-current

problems: IEEE Transactions on Magnetics, **35**, 4452–4458.
Kuzuoglu, M., and R. Mittra, 1996, Frequency dependence of the constitutive parameters of causal perfectly matched anisotropic absorbers: IEEE Microwave and Guided Wave Letters, **6**, 447–449.
Liu, Q., and J. Tao, 1997, The perfectly matched layer for acoustic waves in absorptive media: Journal of the Acoustical Society of America, **102**, 2072–2082.
Luebbers, R. J., and F. Hunsberger, 1992, FDTD for Nth-order dispersive media: IEEE Transactions on Antennas and Propagation, **40**, 1297–1301.
Lysmer, J., and L. A. Drake, 1972, A finite element method for seismology, *in* B. Alder, S. Fernbach, and B. A. Bolt, eds., Methods in computational physics, vol. 11: Academic Press, 181–216.
Ma, S., and P. Liu, 2006, Modeling of the perfectly matched layer absorbing boundaries and intrinsic attenuation in explicit finite-element methods: Bulletin of the Seismological Society of America, **96**, 1779–1794.
Madariaga, R., 1976, Dynamics of an expanding circular fault: Bulletin of the Seismological Society of America, **65**, 163–182.
Marfurt, K. J., 1984, Accuracy of finite-difference and finite-element modeling of the scalar and elastic wave equation: Geophysics, **49**, 533–549.
Martin, R., and D. Komatitsch, 2006, An optimized convolution-perfectly matched layer (C-PML) absorbing technique for 3D seismic wave simulation based on a finite-difference method: Geophysical Research Abstracts, 8, 03988.
Martin, R., D. Komatitsch, and H. Barucq, 2005, An optimized convolution-perfectly matched layer (C-PML) absorbing technique for 3D seismic wave simulation based on a finite-difference method: American Geophysical Union, 86, Abstract NG43B–0574.
Moczo, P., J. Kristek, and E. Bystrický, 2001, Efficiency and optimization of the 3-D finite-difference modeling of seismic ground motion: Journal of Computational Acoustics, **9**, 593–609.
Peng, C. B., and M. N. Töksoz, 1995, An optimal absorbing boundary condition for elastic wave modeling: Geophysics, **60**, 296–301.
Priolo, E., J. M. Carcione, and G. Seriani, 1994, Numerical simulation of interface waves by high-order spectral modeling techniques: Journal of the Acoustical Society of America, **95**, 681–693.
Qi, Q., and T. L. Geers, 1998, Evaluation of the Perfectly Matched Layer for computational acoustics: Journal of Computational Physics, **139**, 166–183.
Quarteroni, A., A. Tagliani, and E. Zampieri, 1998, Generalized Galerkin approximations of elastic waves with absorbing boundary conditions: Computer Methods in Applied Mechanics and Engineering, **163**, 323–341.
Rahmouni, A. N., 2004, Un modèle PML bien posé pour l'élastodynamique anisotrope: Comptes rendus de l'Académie des sciences Paris, Ser. I, 338, 963–968.
Roden, J. A., and S. D. Gedney, 2000, Convolution PML (CPML): An efficient FDTD implementation of the CFS-PML for arbitrary media: Microwave and Optical Technology Letters, **27**, 334–339.
Sánchez-Sesma, F. J., and M. Campillo, 1991, Diffraction of *P*, *SV* and Rayleigh waves by topographic features: A boundary integral formulation: Bulletin of the Seismological Society of America, **81**, 2234–2253.
Sochacki, J., R. Kubichek, J. George, W. R. Fletcher, and S. Smithson, 1987, Absorbing boundary conditions and surface waves: Geophysics, **52**, 60–71.
Stacey, R., 1988, Improved transparent boundary formulations for the elastic wave equation: Bulletin of the Seismological Society of America, **78**, 2089–2097.
Sullivan, D. M., 1997, An unsplit step 3-D PML for use with the FDTD method: IEEE Microwave and Guided Wave Letters, **7**, 184–186.
Teixeira, F. L., and W. C. Chew, 1999, On causality and dynamic stability of perfectly matched layers for FDTD simulations: IEEE Transactions on Microwave Theory and Techniques, **47**, 775–785.
Tessmer, E., and D. Kosloff, 1994, 3-D elastic modeling with surface topography by a Chebyshev spectral method: Geophysics, **59**, 464–473.
Veihl, J. C., and R. Mittra, 1996, An efficient implementation of Bérenger's perfectly matched layer (PML) for finite-difference time-domain mesh truncation: IEEE Microwave and Guided Wave Letters, **6**, 94–96.
Virieux, J., 1986, *P*-*SV* wave propagation in heterogeneous media: velocity-stress finite-difference method: Geophysics, **51**, 889–901.
Wang, T., and X. Tang, 2003, Finite-difference modeling of elastic wave propagation: A nonsplitting perfectly matched layer approach: Geophysics, **68**, 1749–1755.
Winton, S. C., and C. M. Rappaport, 2000, Specifying PML conductivities by considering numerical reflection dependencies: IEEE Transactions on Antennas and Propagation, **48**, 1055–1063.
Yee, K. S., 1966, Numerical solution of initial boundary value problems involving Maxwell's equations: IEEE Transactions on Antennas and Propagation, **14**, 302–307.
Zeng, Y. Q., J. Q. He, and Q. H. Liu, 2001, The application of the perfectly matched layer in numerical modeling of wave propagation in poroelastic media: Geophysics, **66**, 1258–1266.
Zhao, L., and A. C. Cangellaris, 1996, GT-PML: Generalized theory of perfectly matched layers and its application to the reflectionless truncation of finite-difference time-domain grids: IEEE Transactions on Microwave Theory and Techniques, **44**, 2555–2563.